

# Structure of [0001] tilt boundaries in GaN obtained by simulation with empirical potentials

Antoine Béré and Anna Serra\*

*Department de Matemàtica Aplicada III, Escola Tècnica Superior Enginyeria de Camins, Canals i Ports, Universitat Politècnica de Catalunya, Jordi Girona 1-3, 08034 Barcelona, Spain*

(Received 22 April 2002; revised manuscript received 18 June 2002; published 30 August 2002)

The atomic structures of [0001] tilt boundaries from  $9.3^\circ$  to  $44.8^\circ$  misorientation angles in wurtzite gallium nitride have been studied by atomic computer simulation using two interatomic potentials of the Stillinger-Weber and shell-model types. For each misorientation of the two adjacent crystals several periodic boundaries have been considered. A relation between the boundary structures and the cores of the prism **a**-edge dislocation has been established. The structures of some boundaries of larger periods found experimentally have been investigated, and it was found that in some cases they are energetically more favorable than the boundaries of shortest period.

DOI: 10.1103/PhysRevB.66.085330

PACS number(s): 61.72.Mm, 61.72.Bb

## I. INTRODUCTION

GaN is a semiconductor that presents a high applicability in optoelectronics and in high-power, high-frequency devices. However, a significant density of extended defects (threading dislocations, grain boundaries,...) is observed in the grown GaN and some of them are detrimental to the performance of the device. When the growth is produced on the (0001) surface of the substrate and the mosaic growth mode applies, individual islands rotated around the [0001] axis<sup>1</sup> are formed. The misorientation between these islands gives rise to a tilt boundary formation that is often associated with electronic states in covalent semiconductors. Thus, it is important to know their atomic structure from which we can determine whether the electronic states are caused by the intrinsic structural features of the boundary, or by impurities segregated to the boundary. Recently, high-resolution electron microscopy (HREM) images of periodic interfaces such as the symmetric  $\Sigma 19$ ,  $\Sigma 7$ , and  $\Sigma 13$  and asymmetric  $\Sigma 7$  tilt boundaries have been reported.<sup>1</sup> There is experimental evidence that these boundaries contain  $\frac{1}{3}[2\bar{1}\bar{1}0]$  edge dislocations. In a recent paper<sup>2</sup> we presented a preliminary study by atomic computer simulation of some periodic boundaries related to the  $\Sigma 19$ ,  $\Sigma 7$ , and  $\Sigma 13$  coincident site lattice. The procedure of creating the bicrystal and considerations of the possible initial configurations were described there.

In this paper we present the atomic structure of several tilt boundaries of low and high angles of misorientation. We show that the structural units associated to all of them can be explained in terms of combinations of the three stable cores of the  $\frac{1}{3}[2\bar{1}\bar{1}0]$  edge dislocation, namely, the  $\frac{5}{7}$  channel, 4 channel, and 8 channel.<sup>2-3</sup> Two empirical potentials have been used, a modified Stillinger-Weber (SW) and shell-model potential. The SW potential was previously used in the study of **a** and **c** dislocations in GaN.<sup>3</sup>

## II. COMPUTATIONAL METHOD

The simulated system is a bicrystal with a periodic interface containing up to 4000 relaxable atoms. Periodic boundaries were applied in the directions along the interface, whereas in the direction perpendicular to the interface the

boundary was considered periodic if there is an antimirror symmetry perpendicular to the interface,<sup>2</sup> otherwise the boundary was fixed. We notice that the application of the shell model imposes periodic boundaries in all directions. The relaxation procedure is a combination of the conjugate gradient method and the quench-molecular dynamic method. The relaxation finished when the temperature was smaller than  $10^{-6}$  K (SW calculations) or when the gradient norm falls below a certain tolerance (shell-model calculations).<sup>4</sup> The details of the computational methods can be found in Ref. 2 for the tilt boundary model and in Refs. 3–6 for the interatomic potentials.

### A. Tilt boundary model

Let us consider two crystals, white ( $\lambda$ ) and black ( $\mu$ ), initially superimposed. Let us rotate by an angle  $\alpha$  the white crystal anticlockwise around a [0001] axis that passes through an atomic site. The obtained dichromatic complex has certain atoms in coincidence that forms a superlattice, namely, the coincident site lattice (CSL) that is common to the two crystals (see Fig. 1). The interface plane of the bicrystal is chosen among the planes of the CSL. Figure 1 shows the two planes chosen in our work for the  $\Sigma 19$ . The bicrystal is created by discarding the white crystal from the one side of the chosen plane and the black crystal from the other side. The CSL is characterized by the multiplicity  $\Sigma$  (ratio between the volume of the unit cells of the CSL and the crystal lattice). In the case of the hexagonal symmetry, there are two different angles of rotation ( $\alpha_1$  and  $\alpha_2$ ) about the **c** axis that lead to the same CSL (see Ref. 7, Appendix A). They are related by  $\alpha_1 + \alpha_2 = 60^\circ$ . In Table II the rotation angles of minimum value  $\alpha_{\min}$  for the interfaces studied are listed. For a given crystallographic plane of the CSL (i.e., for a given interface), the angle  $\theta$  formed by the  $(11\bar{2}0)_\lambda$  and  $(11\bar{2}0)_\mu$  planes closer to the interface (see Fig. 1) coincides either with  $\alpha_1$  or  $\alpha_2$ . This angle  $\theta$  is defined as the misorientation angle of the interface. In Table II the misorientation angles measured on our simulations are listed. For a given CSL, the misorientation angle is either the rotation angle  $\alpha$  or its complementary to  $60^\circ$ .

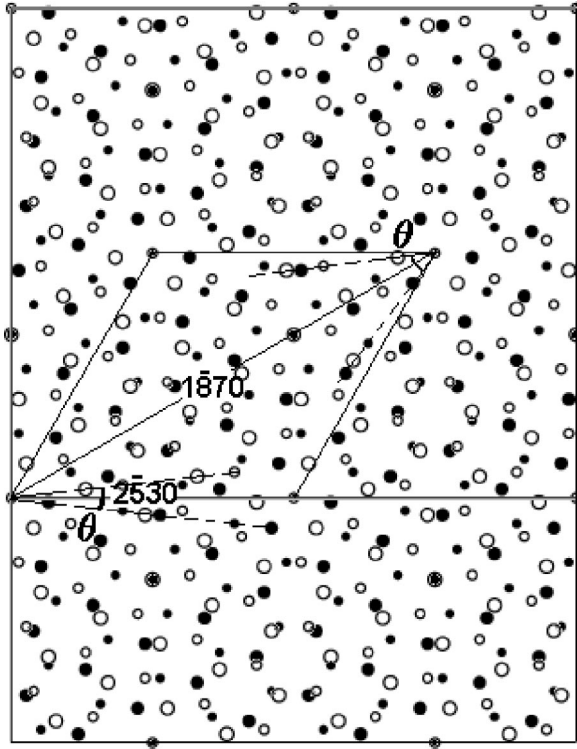


FIG. 1. Dichromatic complex of  $\Sigma 19$ . The two boundaries studied ( $2\bar{5}30$ ) and ( $1\bar{8}70$ ) are shown within a CSL unit cell. The misorientation angles  $\theta$  for each boundary are indicated. The small circles represent N atoms in A sites of the wurtzite lattice, big circles represent Ga atoms in B sites. Notice that one small circle superimposed one big circle and vice versa.

When the crystals exhibit an  $n$ -atom basis, the bottom surface of the upper crystal (assumed to be  $\lambda$ ) can be terminated at  $n$  different levels thereby leading to  $n$  distinguishable unrelaxed surfaces. The same situation arises to the  $\mu$  crystal. In the present study, limited to  $[0001]$  tilt boundaries, there are two possible levels ( $a$  and  $b$  type) corresponding to the two basal planes. Thus, there are four possible interfaces  $a(\lambda)/a(\mu)$ ,  $a(\lambda)/b(\mu)$ ,  $b(\lambda)/a(\mu)$ , and  $b(\lambda)/b(\mu)$ , although symmetries can reduce the total number to be considered. Once the interface is constructed, the relative displacements parallel to the interface that can produce different configurations are considered. These displacements in a periodic boundary are confined to a Wigner-Seitz cell, i.e., the cell of nonidentical displacements (CNID).<sup>8</sup> Therefore, distinct CNID's should be considered for each interface except in the interfaces that contain both  $a$ - and  $b$ -type atoms, then a unique CNID exists.<sup>9</sup> This is, for example, the case of the symmetric boundary  $\Sigma 13$  along the  $(2\bar{7}50)$  plane.

In each CNID the configurations that correspond to structures of a local minimum energy were identified in the corresponding  $\gamma$  surface calculated applying relative displacements of the two half crystals parallel to the boundary. In some cases a displacement along the  $c$  direction restores locally the environment of the perfect crystal reducing significantly the surface energy.

TABLE I.  $\Sigma 19$  ( $2\bar{5}30$ ) tilt boundary energy as a function of interatomic potentials. Two sets of parameters have been used for the description of the shell model. More detailed descriptions of atomic structures exhibiting the  $\frac{5}{7}$ - and 4-atom rings are given in a previous paper [see Ref. 2, Figs. 5(a) and 5(b)].

Structure	Energy (mJ/m <sup>2</sup> )	
	Stillinger-Weber	Shell model
$\frac{5}{7}$	1518	2078 <sup>a</sup> 2073 <sup>b</sup>
4	1806	2014 <sup>a</sup> 2051 <sup>b</sup>
8	1934	1958 <sup>a</sup> 1963 <sup>b</sup>

<sup>a</sup>Using shell model parameters given by Zapol, Pandey, and Gale (Ref. 5).

<sup>b</sup>Using shell model parameters given by Chisholm, Lewis, and Bristowe (Ref. 6).

### B. Interatomic potential

The potential model used is an empirical potential of Stillinger-Weber type that was previously used for the calculation of atomic structures in semiconductors.<sup>10-12</sup> It has been adapted to take into account the different possible interactions in GaN, namely, Ga-N, Ga-Ga, and N-N.<sup>3,13</sup> We have used this potential in the simulation of the cores of crystal dislocations in GaN obtaining core structures in accordance with the HREM observations.<sup>1</sup>

In order to study the influence of the potential on the simulated structures and energies, we have also used another empirical potential, the shell model.<sup>4</sup> This model consists of a long-range Coulombic term and a short-range interaction of Buckingham form. The polarization of nitrogen atoms is considered by modeling the electrons with a massless shell harmonically coupled to the core. This potential is more suitable for GaN than the SW model because it considers the partly ionic character of this material. However, it is more expensive in calculation time and it is restricted to simulations with periodic boundary conditions. Therefore we used the SW potential for the calculation of the  $\gamma$  surfaces of each CNID. The identified configurations of low energy are then relaxed using the shell model in order to check if the structure conserves its geometry and to calculate the boundary energy.

It was found that the shell model does not introduce new (other than the  $\frac{5}{7}$ , 4, and 8) structural units. The shell model gives no strongly preferred structure whereas the Stillinger-Weber potential yields a clear structural minimum ( $\frac{5}{7}$ ), which is actually the highest in energy using the shell model. In Table I the energies of the three structural units calculated with both potentials are presented for the  $\Sigma 19$  boundary.

### III. RESULTS

The atomic structures and the values of the energies that will be presented in the following have been obtained with the SW empirical potential. A variety of  $[0001]$  tilt boundaries with misorientation angles from  $\theta=9.3^\circ$  (corresponding to  $\Sigma 37$ ) to  $\theta=44.8^\circ$  (corresponding to  $\Sigma 43$ ) have been simulated. There are experimental images for most of the boundaries studied, some of them have been found in GaN (Ref. 1) and the others in materials of wurtzite structure.<sup>7,14</sup>

TABLE II. The data for [0001] tilt boundaries.  $\alpha_{\text{calc}}$  corresponds to the rotation angle calculated in the low angle approximation,  $\alpha_{\text{min}}$  is the minimum rotation angle given in Ref. 15 and  $\Delta\alpha$  their deviation. The angle  $\theta$ , measured in the simulated boundaries, refers to the misorientation angle.  $\Delta E$  is the lower structure energy. The length of period vectors along the interfaces ( $T$ ) and the total Burgers vector ( $b$ ) in the low angle approximation are given in lattice parameter units.

$\Sigma$	Indices	$b(a)$	$T(a)$	$\alpha_{\text{calc}}$	$\alpha_{\text{min}}$	$\Delta\alpha$ (%)	$\theta$	$\Delta E$ (mJ/m <sup>2</sup> )
37	(3 $\bar{7}$ 40)	1	$\sqrt{37}$	9.3	9.3	3	9.3	1286
19	(2 $\bar{5}$ 30)	1	$\sqrt{19}$	12.9	13.2	3	13.4	1518
	(1 $\bar{8}$ 70)	$\sqrt{3}$	$\sqrt{57}$				46.6	1757
31	(1 $\bar{6}$ 50)	$\sqrt{3}$	$\sqrt{31}$	17.3	17.9	3	42.2	2062
	( $\bar{7}$ 1 1 $\bar{4}$ 0)	3	$\sqrt{93}$				17.8	1447
49	(3 $\bar{8}$ 50)	2	$\sqrt{49}$	16.0	16.4	3	16.3	1692
13	(1 $\bar{4}$ 30)	$\sqrt{3}$	$\sqrt{13}$	25.7	27.8	8	32.2	1528
	(2 $\bar{7}$ 50)	3	$\sqrt{39}$				27.8	2185
7	(1 $\bar{3}$ 20)	1	$\sqrt{7}$	20.7	21.8	4	21.6	1827
	(0 $\bar{1}$ 10)	$\sqrt{7}$	$\sqrt{49}$				38.4	1642
43	(1 $\bar{7}$ 60)	$\sqrt{3}$	$\sqrt{43}$	14.8	15.2	3	44.8	1834

It follows a description of their atomic structure and some energetic considerations. As a general trend, all structural units can be related to the structures of the cores of the  $\mathbf{a}$  edge dislocation. These cores have been previously studied with the same SW potential,<sup>3</sup> giving three possible stable structures formed by  $\frac{5}{7}$  channels, 4 channels, and 8 channels, respectively, the  $\frac{5}{7}$  core being the one of lowest energy. This core is related to a line dislocation located in the widely spaced  $\{1\bar{1}00\}$  glide planes whereas the 4 and 8 cores are related to a line dislocation located in the narrow spaced planes.

Table II gives the crystallographic parameters and lower-energy structures of the bicrystals studied. There is not a clear relationship between the energy and other characteristics of the boundary such as the misorientation, the periodic distance along the direction  $\mathbf{T}$  perpendicular to the [0001] direction or the number and shape of the channels that form the structural unit. Therefore, in this section we present two classifications. On the one hand, we have grouped the boundaries according to the relative surface energy; we distinguish three groups, i.e., the boundaries of low energy and low angle of misorientation, the boundaries of highest energy, and all the others. On the other hand, we present an alternative grouping by considering the composition of the structural units.

#### A. Low-misorientation-angle–low-energy boundaries

The low angle tilt boundaries are formed by arrays of edge dislocations, in accordance with the description of simple dislocation boundaries. We consider in this group misorientation angles of 9.3°, 13.2°, and 17.8°.

The  $\Sigma 37$  boundary with a misorientation of  $\theta = 9.3^\circ$  and boundary plane (3 $\bar{7}$ 40) and the  $\Sigma 19$  boundary with a misorientation of  $\theta = 13.2^\circ$  and boundary plane (2 $\bar{5}$ 30) have similar characteristics. In both cases, the boundary of minimum

energy corresponds to a configuration of the  $a(\lambda)/b(\mu)$  or the  $b(\lambda)/a(\mu)$  type, where the structural unit is the  $\frac{5}{7}$  channel [Figs. 2(a)–2(d)], whereas the  $a(\lambda)/a(\mu)$  and  $b(\lambda)/b(\mu)$  types present a single stable configuration with a four-channel structure [Fig. 2(e)].

Figure 2(a) shows the configuration of minimum energy (1286 mJ/m<sup>2</sup>) of the  $\Sigma 37$ . It is formed by one dislocation of  $\frac{5}{7}$  type per period,  $\mathbf{T} = \frac{1}{3}[11, \bar{1}0, \bar{1}, 0]$ , which gives a linear density of dislocations along  $\mathbf{T}$  of 0.05 Å<sup>-1</sup>. Taking one of the single crystals as reference, the corresponding Burgers vector of the dislocation is  $\mathbf{b}_1 = \frac{1}{3}[\bar{1}\bar{1}20]$ . In the bicrystal the Burgers vector is perpendicular to the boundary and the approximation for the low angle boundaries, i.e.,  $\text{tg}\alpha = |b|/|T|$ , is accomplished. Three other stable configurations of higher energy exist (1920, 2071, and 2209 mJ/m<sup>2</sup>) which are related to the previous one by a translation  $\varepsilon\mathbf{T}$  ( $0 < \varepsilon < 1$ ). Figures 2(b)–2(d) show that their structural units are formed by two  $\frac{5}{7}$  dislocations with Burgers vectors  $\mathbf{b}_2$  and  $\mathbf{b}_3$ , where  $\mathbf{b}_2 + \mathbf{b}_3 = \mathbf{b}_1$ . The fact that double amount of dislocations accommodate the same misorientation explains the increase in energy. Figure 2(e) shows the boundary formed by 4 channels. The energy per unit area of this boundary is 1485 mJ/m<sup>2</sup>. The energy of the 4-channel configuration is higher than the energy of the  $\frac{5}{7}$ -channel configuration in accordance to the energies of the corresponding edge dislocation cores.<sup>3</sup>

The  $\Sigma 19$  boundary along the plane (2 $\bar{5}$ 30) with a misorientation of  $\theta = 13.2^\circ$  follows the same pattern as the  $\Sigma 37$ . This plane presents the shorter period  $\mathbf{T}_1 = \frac{1}{3}[\bar{8}710]$  and the configuration of lowest energy (1518 mJ/m<sup>2</sup>) corresponds to a structural unit of one  $\frac{5}{7}$  channel (for more detailed description, see Ref. 2). A second  $\Sigma 19$  boundary of larger period along the plane (1 $\bar{8}$ 70) is shown in Fig. 3. The period is  $\mathbf{T}_2 = \frac{1}{3}[\bar{1}5, 6, 9, 0]$  and it is formed by two  $\frac{5}{7}$  channels of Burgers vectors  $\mathbf{b}_1$  and  $\mathbf{b}_2$  that provide a total Burgers vector

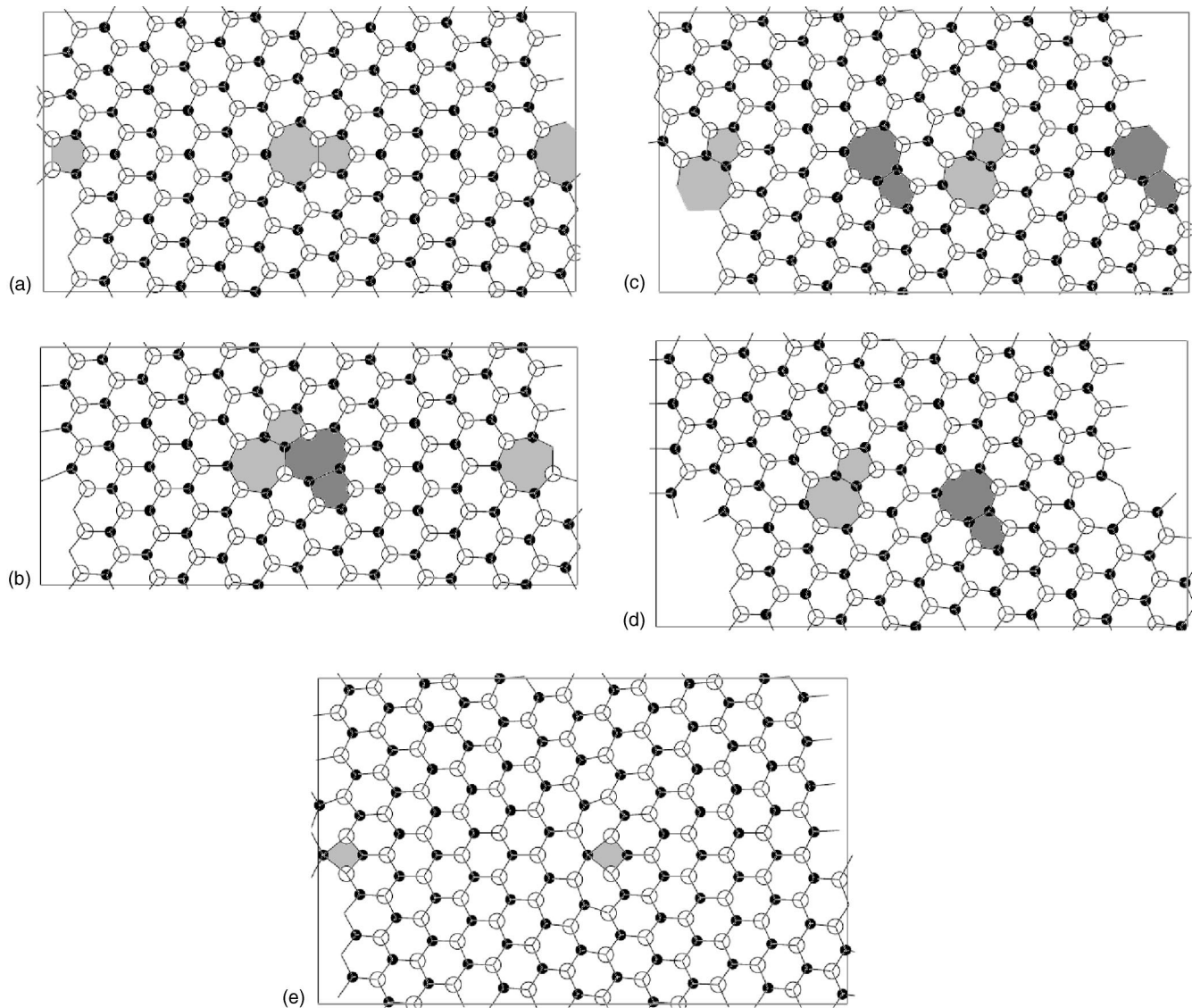


FIG. 2. Atomic structures of the  $\Sigma 37$  ( $\theta=13.4^\circ$ ) ( $3\bar{7}40$ ) tilt boundary. The closed circles represent N atoms in A sites of the wurtzite lattice, open circles represent Ga atoms in B sites. Notice that one closed circle superimposed one open circle and vice versa. The structures in (a) and (e) correspond to  $a(\lambda)/b(\mu)$  and  $b(\lambda)/b(\mu)$  configurations, respectively. The structures in (b), (c), and (d) correspond to translation states of the  $a(\lambda)/b(\mu)$  starting configuration. The structure in (a) is the most energetically favorable.

$[0\bar{1}10]$ . In this case the energy is  $1757 \text{ mJ/m}^2$ . The components of  $\mathbf{b}_1$  and  $\mathbf{b}_2$  parallel to the boundary cancel each other but they contribute to the increase in the energy of the boundary. In both  $\Sigma 19$  boundaries the low angle boundary approximation gives the same rotation angle of  $12.9^\circ$ .

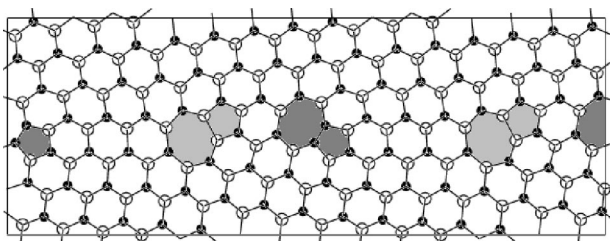


FIG. 3. Atomic structure of the lower-energy  $\Sigma 19$  ( $\theta=46.6^\circ$ ) ( $1\bar{8}70$ ) tilt boundary.

In the same group we have included the  $\Sigma 31$  boundary with a misorientation of  $\theta=17.8^\circ$  and boundary plane ( $7\bar{1}1\bar{4}0$ ). Although the angle is not small, this boundary has low energy and the structural units can be described as in the previous cases. The configuration of minimum energy ( $1447 \text{ mJ/m}^2$ ) is formed by a set of three  $\frac{5}{7}$  channels within a period  $\mathbf{T}=[5\bar{6}10]$ , as shown in Fig. 4(a). By creating a Burgers circuit around one of the  $\frac{5}{7}$  channels and taking one of the crystals as reference it is still possible to identify it as an edge dislocation. Thus, the total effective Burgers vector per period is  $3\mathbf{a}$  and the associated rotation angle within the low angle approximation is  $17.3^\circ$  with an error  $\Delta\alpha=0.5^\circ$  (2.8%). Figure 4(b) shows a HREM image<sup>14</sup> of the same boundary in AlN. Based solely on a geometrical model, Potin and co-workers described the boundary as formed by two different channels ( $\frac{5}{7}$  and 8). With energetic calculations, the com-

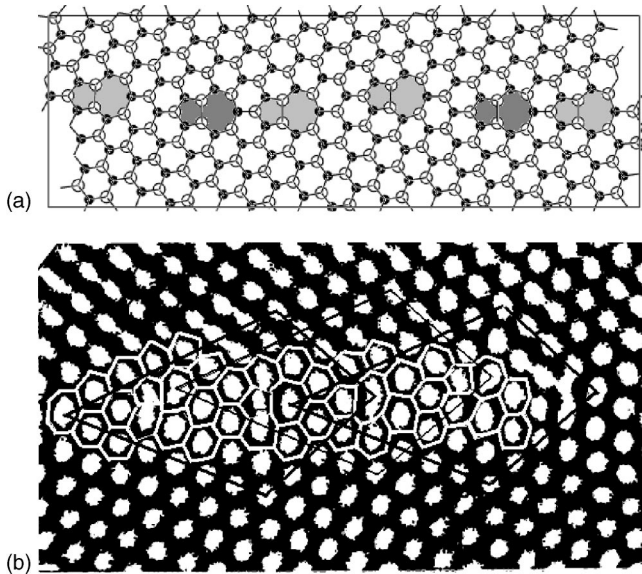


FIG. 4. (a) Atomic structure of the lower-energy  $\Sigma_{31}$  ( $\theta = 17.8^\circ$ ) ( $\bar{4}11\bar{7}0$ ) tilt boundary. (b) High-resolution micrograph of the  $\Sigma_{31}$  ( $\theta = 17.8^\circ$ ) ( $\bar{4}11\bar{7}0$ ) tilt boundary in AlN (Ref. 14).

parison between the simulated boundary and the experimental image allows a more accurate identification of the atomic structure of the boundary, especially in such places where the local distortion associated to the channels does not give a clear image. The simulation shows that the structure of lower energy of this boundary is described with only one type of channels, i.e.,  $\frac{5}{7}$  channels according to the SW potential.

Unlike the boundaries presented above, the  $\Sigma_{49}$  boundary with a misorientation of  $\theta = 16.3^\circ$  and boundary plane ( $3\bar{8}50$ ) cannot be accommodated solely by  $\frac{5}{7}$  channels. It is formed by one  $\frac{5}{7}$  and one 4 channel equally distributed in a period of  $\mathbf{T} = \frac{1}{3}[13, \bar{11}, \bar{2}, 0]$  as shown in Fig. 5. We have included this boundary in the group of low angle boundaries because of the reasonable agreement with the low angle approximation ( $\alpha = 16.0^\circ$ , 3% of error). The energy per unit area is  $1692 \text{ mJ/m}^2$ . The reason for which this energy is bigger than that associated with the misorientation of  $\theta = 17.8^\circ$  is because the present boundary has a 4 channel which has bigger energy than the  $\frac{5}{7}$  channel (at least within the SW potential).

### B. Tilt boundaries of high energy

We describe in this section the boundaries that in the most stable configuration present the highest energies (above 2000

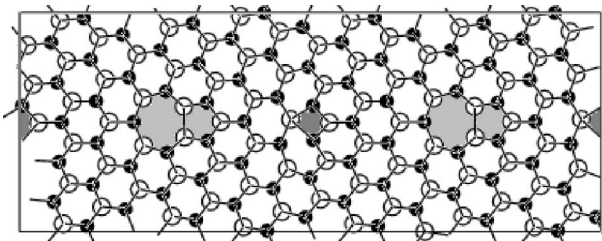


FIG. 5. Atomic structure of the lower-energy  $\Sigma_{49}$  ( $\theta = 16.3^\circ$ ) ( $3\bar{8}\bar{5}0$ ) tilt boundary.

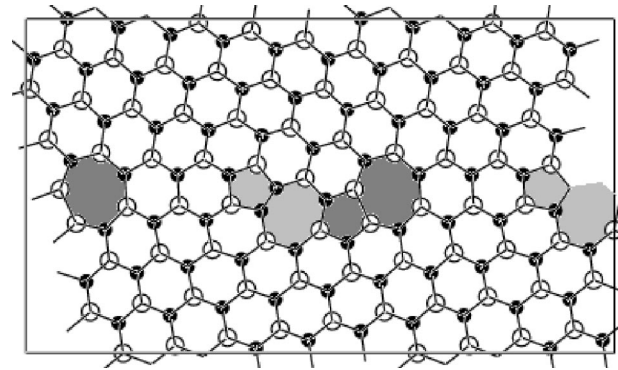


FIG. 6. Atomic structure of the lower-energy  $\Sigma_{31}$  ( $\theta = 42.2^\circ$ ) ( $1\bar{6}\bar{5}0$ ) tilt boundary.

$\text{mJ/m}^2$ ). This is the case of the second boundary studied for the  $\Sigma_{31}$  CSL along the plane ( $1\bar{6}\bar{5}0$ ) and misorientation  $\theta = 42.2^\circ$  (see Fig. 6). It has a shorter period ( $\mathbf{T} = \frac{1}{3}[\bar{1}\bar{1}, 7, 4, 0]$ ) but higher energy ( $2062 \text{ mJ/m}^2$ ), compared with the  $\Sigma_{31}$  boundary described in Sec. III A. In this case the angle of rotation  $\alpha = 17.8^\circ$  has to be accommodated by an effective total dislocation with a Burgers vector equal to  $\alpha\sqrt{3}$ . This is achieved by two  $\frac{5}{7}$  channels oriented such that the sum of their Burgers vectors is of the  $[1\bar{1}00]$  type. The increase in energy is due to the fact that the dislocations have components of the Burgers vectors parallel to the boundary that although cancel each other but contribute to the total energy. The same situation is found in  $\Sigma_{19}$  (Fig. 3).

The  $\Sigma_{13}$  boundary with a misorientation of  $\theta = 27.8^\circ$  and boundary plane ( $2\bar{7}50$ ) has the highest energy among the studied boundaries ( $2185 \text{ mJ/m}^2$ ). The plane ( $2\bar{7}50$ ) contains atoms of both “a” and “b” types and therefore only one CNID exists. Figure 7(a) shows the relaxed configuration of minimum energy which is formed by three  $\frac{5}{7}$  channels along  $\mathbf{T} = [3\bar{4}10]$ . In this case the low angle approximation would assign a misorientation of  $25.7^\circ$  (8% of error) indicating that this boundary cannot be understood as the superposition of crystal dislocations in a single crystal. This structure is in agreement with the experimental micrographs in ZnO.<sup>7</sup> Under a relative translation of the crystals along  $\frac{5}{7}\mathbf{T}$ , another configuration formed by a structural unit of  $8\frac{5}{7}$ -4 channels can be found [see Fig. 7(b)]. However, it has higher energy due to the big distortions of the bonds around the 4 channel.

### C. Other tilt boundaries

As for  $\Sigma_{31}$ , in the case of  $\Sigma_{13}$  we have also studied another plane with shorter period, i.e., the ( $1\bar{4}30$ ) plane and misorientation  $\theta = 32.2^\circ$  (see Fig. 8) where  $\mathbf{T} = \frac{1}{3}[\bar{7}250]$ . The most stable configuration ( $1528 \text{ mJ/m}^2$ ) is formed by units of two  $\frac{5}{7}$  channels alternatively oriented and arranged in a continuous way forming a corrugated interface. This structure was found experimentally in ZnO.<sup>7</sup>

Two boundaries have been studied for  $\Sigma_7$  CSL and minimum rotation angle  $\alpha = 21.79^\circ$ . The first along the ( $1\bar{3}20$ ) plane, is symmetric and has a misorientation  $\theta = 21.6^\circ$  and a

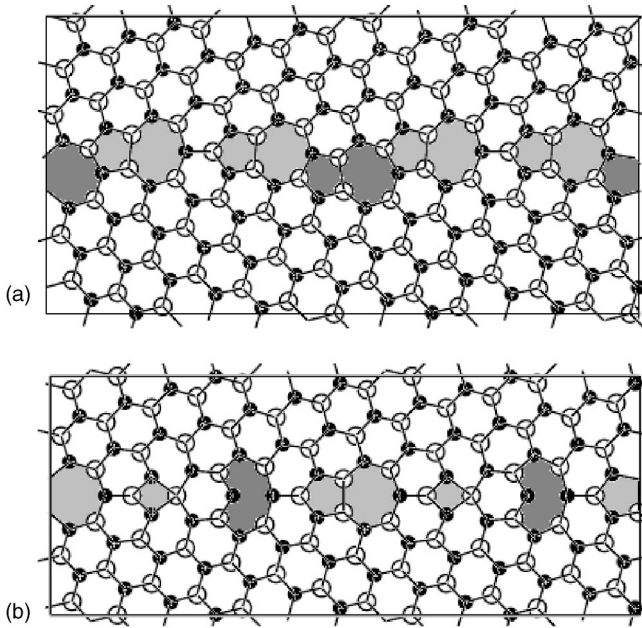


FIG. 7. Atomic structures of the  $\Sigma_{13}$  ( $\theta=27.8^\circ$ )  $2\bar{5}70$  tilt boundary. The interface plane comprises both  $a$ - and  $b$ -type atoms. The structure in (a) corresponds to a translation state of the structure in (b). The structure in (a) has the smaller energy.

period  $\mathbf{T} = \frac{1}{3}[\bar{5}140]$ . The low angle approximation gives a rotation of  $\alpha = 20.7^\circ$ , with an error of less than 4%. As with the  $\Sigma_{37}$  and  $\Sigma_{19}$  boundaries, two different CNID's exist exhibiting  $\frac{5}{7}$  channels and 4 channels respectively in the stable configurations. The boundary of lower energy ( $1827 \text{ mJ/m}^2$ ) corresponds to a structure with one  $\frac{5}{7}$  channel (for more detailed description see Ref. 2, Fig. 7).

The second boundary (Fig. 9) is asymmetric and it is formed by joining the planes  $(0\bar{1}10)_\lambda$  of the upper crystal and  $(3\bar{8}50)_\mu$  of the lower crystal. The misorientation angle is  $\theta = 38.4^\circ$ . It is formed by three  $\frac{5}{7}$  channels distributed in a period  $\mathbf{T} = \frac{2}{3}[2\bar{1}\bar{1}0]_\lambda \equiv \frac{1}{3}[\bar{1}\bar{3}, 2, 11, 0]_\mu$ . The energy of the configuration shown in Fig. 9 is  $1642 \text{ mJ/m}^2$ .

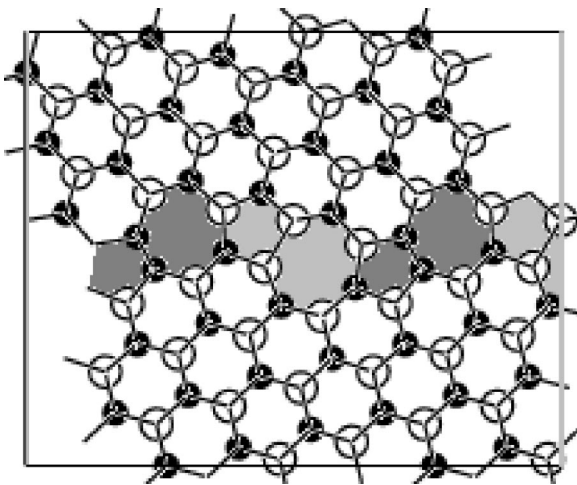


FIG. 8. Atomic structures of the lower-energy  $\Sigma_{13}$  ( $\theta=32.2^\circ$ )  $(1\bar{4}30)$  tilt boundary.

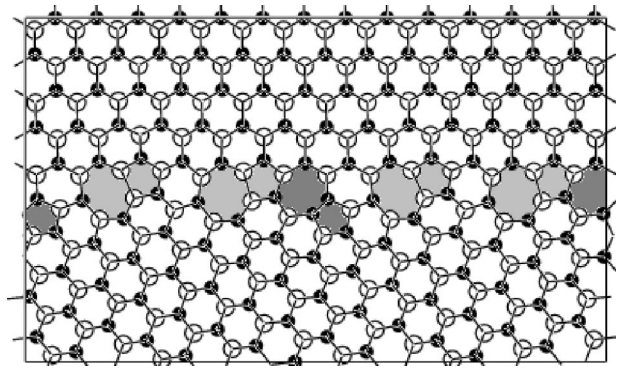


FIG. 9. Atomic structure of the lower-energy  $\Sigma_7$  ( $\theta=38.4^\circ$ )  $(0\bar{1}10)/(3\bar{8}50)$  tilt boundary.

Finally we consider the  $\Sigma_{43}$  CSL with a minimum rotation angle  $\alpha = 15.2^\circ$ . The boundary chosen is along the  $(1\bar{7}60)$  plane and has a misorientation angle of  $\theta = 44.8^\circ$ . Figure 10 shows the configuration of lower energy ( $1834 \text{ mJ/m}^2$ ) formed by two  $\frac{5}{7}$  channels in a period  $\mathbf{T} = [\bar{1}\bar{3}, 5, 8, 0]$ . Their orientations provide total Burgers vector of the  $[01\bar{1}0]$  type and would accommodate an angle of  $14.8^\circ$  within the low angle boundary model.

#### D. Summary about the structural units

The structural units of the stable tilt boundaries can be described in terms of the three stable cores of the prism  $a$ -edge dislocation.<sup>2-3</sup> Thus, the boundary structures can be classified into three groups according to the combination of these units.

The first group is composed of boundaries with only one type of  $n$ -coordinated channel, i.e.,  $\Sigma_{37}$  ( $3\bar{7}40$ ),  $\Sigma_{19}$  ( $2\bar{5}30$ ), and  $\Sigma_7$  ( $1\bar{3}20$ ). We obtained that the configurations of  $a(\lambda)/b(\mu)$  type give rise to interfaces with  $\frac{5}{7}$ -coordinated channels [Fig. 2(a)], whereas configurations of  $b(\lambda)/b(\mu)$  type give rise to interfaces with 4-coordinated channels [Fig. 2(e)]. Other interfaces corresponding to translation states of the  $a(\lambda)/b(\mu)$  type are obtained and exhibit two  $\frac{5}{7}$ -coordinated channels of alternate orientations [Figs. 2(b) and 2(d)]. For this group, the  $\frac{5}{7}$  interface is the structure of lower energy in agreement with the experimental results.<sup>1</sup>

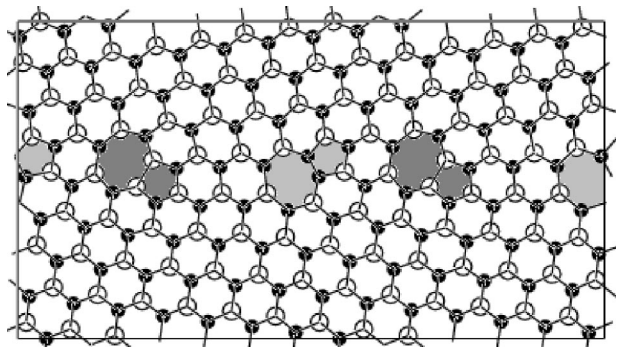


FIG. 10. Atomic structure of the lower-energy  $\Sigma_{43}$  ( $\theta=44.8^\circ$ )  $(1\bar{7}60)$  tilt boundary.

The second group is composed of planar boundaries that contain at least two types of  $n$ -coordinated channels, i.e.,  $\Sigma 49$  ( $3\bar{8}50$ ),  $\Sigma 13$  ( $1\bar{4}30$ ), and  $\Sigma 13$  ( $2\bar{7}50$ ). They also give rise to corrugated interfaces corresponding to translations states with  $\frac{5}{7}$ -atom rings of alternate orientations (Figs. 5, 7, and 8). Our calculations show that they are energetically more favorable than the planar interfaces. Kiselev and co-workers give experimental evidence of these boundaries in ZnO.<sup>7</sup>

The third group is formed by boundaries such that the most stable configuration contains at least two  $\frac{5}{7}$  channels, i.e.,  $\Sigma 7$  ( $0\bar{1}10$ )/( $3\bar{8}50$ ),  $\Sigma 19$  ( $1\bar{8}70$ ),  $\Sigma 31$  ( $1\bar{6}50$ ),  $\Sigma 31$  ( $4\bar{1}\bar{1}70$ ), and  $\Sigma 43$  ( $1\bar{7}60$ ). Experimental evidence is given in Refs. 1 and 7.

#### IV. SUMMARY AND CONCLUDING REMARKS

We have simulated [0001] tilt boundaries from  $9.3^\circ$  to  $44.8^\circ$  misorientation angles using an empirical potential of Stillinger-Weber type and the shell model. For each boundary we have considered the different possible cells of non-identical displacements and we have calculated the corresponding  $\gamma$  surfaces to search all possible stable configurations. In all boundaries the structural units are formed by combinations of  $\frac{5}{7}$ -, 4-, and/or 8-coordinated channels. No other stable atomic structures were found either with the SW potential or with the shell-model potential. Other structures reported previously<sup>16–17</sup> in other materials of wurtzite structure are related to the ones reported in this work by a relative translation of the crystals along the interface and they present higher energy. Comparing the studied semiconductor to other simpler hexagonal structures, such as pure metals where the energy changes smoothly with the position of the atoms, the strongly directional character of the bonds in GaN limits the rearrangement of the atoms to

structures where the change of bond length and angle is minimized. This limits, in fact, the number of atomic structural units to the three found experimentally and reported here. This could explain the coincidence of the two potentials about the stable structures even if they present different relative energies.

The  $\frac{5}{7}$ -, 4-, and/or 8-coordinated channels have the same atomic structure as the stable cores of the  $a$ -edge dislocation. In fact, boundaries with rotation angles up to  $18^\circ$  can be identified as alignments of  $a$ -edge dislocations since the approximation for the low angle boundaries, i.e.,  $\tan \alpha = |b|/|T|$ , is accomplished within 3% of error.

If a tilt boundary appears as a consequence of the lateral growth of two islands, the rotation angle is fixed and therefore the only variable that can influence the final surface energy is the boundary plane. This may explain the appearance of faceted interfaces where the increase in surface is compensated by the lower energy of the planes of the facets. In some CSL we found that boundaries with large period are more stable than that with smallest period. The energy per unit area is better related to the density of coordinated channels than to the length of the period. Moreover, no clear relationship has been found between energies and misorientation angles. The stable structures are in agreement with the experimental HREM images obtained either in GaN or other crystals of wurtzite structure concerning the  $\Sigma 19$  ( $2\bar{5}30$ ),<sup>1</sup>  $\Sigma 7$  ( $1\bar{3}20$ ),<sup>1</sup>  $\Sigma 7$  ( $0\bar{1}10$ )/( $3\bar{8}50$ ),<sup>1</sup>  $\Sigma 31$  ( $4\bar{1}\bar{1}70$ ),<sup>14</sup>  $\Sigma 13$  ( $1\bar{4}30$ ),<sup>7</sup> and  $\Sigma 13$  ( $2\bar{7}50$ ) (Ref. 7) boundaries.

#### ACKNOWLEDGMENTS

The authors acknowledge the support of the UE (Contract No. HPRN-CT-1999-00040) and the Spanish MCYT (Grant No. BFM2000-0596-C03-03).

\*Email address: a.serra@upc.es

<sup>1</sup>V. Potin, P. Ruterana, G. Nouet, R. C. Pond, and H. Morkoç, Phys. Rev. B **61**, 5587 (2000).

<sup>2</sup>A. Béré and A. Serra, Interface Sci. **9**, 149 (2001).

<sup>3</sup>A. Béré and A. Serra, Phys. Rev. B **65**, 205323 (2002).

<sup>4</sup>J. D. Gale, J. Chem. Soc., Faraday Trans. **93**, 629 (1997).

<sup>5</sup>P. Zapol, R. Pandey, and J. D. Gale, J. Phys.: Condens. Matter **9**, 9517 (1997).

<sup>6</sup>J. A. Chisholm, D. W. Lewis, and P. D. Bristowe, J. Phys.: Condens. Matter **11**, L235 (1999).

<sup>7</sup>A. N. Kiselev, F. Sarrazit, E. A. Stepantsov, E. Olsson, T. Claesson, V. I. Bondarenko, R. C. Pond, and N. A. Kiselev, Philos. Mag. A **76**, 633 (1997).

<sup>8</sup>V. Vitek, A. P. Sutton, D. A. Smith, and R. C. Pond, *Grain Boundary Structure and Kinetics*, edited by R. W. Balluffi (ASM, Metals Park, OH, 1980), p. 115.

<sup>9</sup>R. C. Pond, D. J. Bacon, A. Serra, and A. P. Sutton, Metall. Trans. A **22**, 1185 (1991).

<sup>10</sup>A. S. Nandedkar and J. Narayan, Philos. Mag. A **61**, 873 (1990).

<sup>11</sup>Q. Ren, B. Joós, and M. S. Duesbery, Philos. Mag. A **52**, 13 223 (1995).

<sup>12</sup>H. Koizumi, Y. Kamimura, and T. Suzuki, Philos. Mag. A **80**, 609 (2000).

<sup>13</sup>N. Aïchoune, V. Potin, P. Ruterana, A. Hiarie, G. Nouet, and E. Paumier, Comput. Mater. Sci. **17**, 380 (2000).

<sup>14</sup>V. Potin, A. Béré, P. Ruterana, and G. Nouet, Mater. Sci. Forum **294–296**, 243 (1999).

<sup>15</sup>P. Delavignette, J. Phys. Colloq. **43**, C1-1 (1982).

<sup>16</sup>F. Oba, I. Tanaka, S. R. Nishitani, H. Adahi, B. Slater, and D. H. Gay, Philos. Mag. A **80**, 1567 (2000).

<sup>17</sup>J. M. Carlsson, B. Helsiny, H. S. Domingos, and P. D. Bristowe, J. Phys.: Condens. Matter **13**, 9937 (2001).